Reduction of Rh/CeO_2–ZrO_2 with hydrogen

Keiji Hashimoto [a], Naoji Toukai [a], Rei Hamada [b] and Seiichiro Imamura [b]

[a] *Osaka Municipal Technical Research Institute, Morinomiya, Joto-ku, Osaka 536, Japan*
[b] *Department of Chemistry, Kyoto Institute of Technology, Matsugasaki, Sakyo-ku, Kyoto 606, Japan*

Received 10 September 1997; accepted 10 December 1997

The effects of the addition of rhodium to CeO_2(70 wt%)–ZrO_2 support on hydrogen reduction of the support have been studied. The effects change significantly with an increase in calcination temperature of the support. The lattice constant of CeO_2–ZrO_2 decreases with an increase in calcination temperature. The correlation curve between the lattice constant and calcination temperature as well as that between crystalline growth and calcination temperature has an inflection point at 900°C. Thus, the structure of the CeO_2–ZrO_2 solid solutions depends on the calcination temperature. In particular, the structure changes significantly at 900°C and calcination at 900°C shows a maximum amount of surface oxygen-deficient sites catalyzing N_2O decomposition. Moreover, the reduction extent at 400°C is directly proportional to rhodium concentration per unit surface area in addition to the considerable structure change of CeO_2–ZrO_2. Hence, the localization and/or aggregation effect of rhodium particles also contributes to the reduction creating surface oxygen vacancy.

Keywords: ceria–zirconia, rhodium, reduction, hydrogen

1. Introduction

Ceria has been often used to improve the catalytic properties, such as (1) oxygen storage and release by interchanging between CeO_2 under oxidizing conditions and Ce_2O_3 under reducing conditions [1–12] and (2) stabilization of supported metals and supports [13–16]. The solution of zirconia in ceria increases significantly the oxygen storage action of ceria and thermal stability of supported metals and supports. There are many studies on the correlation between calcination temperature and the structure of CeO_2–ZrO_2 [17–20]. It is known that their crystal phase and ceria structure depend on the extent of the dissolution of zirconium into the ceria due to preparation conditions and that the addition of the metals such as Rh and Pt promotes the formation of oxygen vacancies [21]. In addition, the incorporation of zirconium metal ions in the CeO_2 lattice increases significantly the amount of oxygen vacancies creating Ce^{3+}, which may play a crucial role in enhancing NO and CO conversions [18,22]. The morphology of the precious metal particles and the correlation between the role of the metal and the structure of CeO_2–ZrO_2 still remain obscure, although the morphology and the correlation may contribute importantly to catalytic activity and reduction of ceria creating oxygen-deficient sites. We had studied the application of Rh/CeO_2 to N_2O decomposition and reported that this catalyst was very effective in decomposing N_2O even at low temperature and that the activity was due to the inherent function of rhodium coupled with oxygen-deficient sites in the ceria [23]. However, the number of oxygen-deficient sites in the ceria is insufficient for practical use and the state of rhodium was not clarified. In this work we tried to incorporate zirconia in ceria to increase the amount of oxygen-deficient sites in ceria and its activity. The hydrogen reduction of rhodium oxide supported on CeO_2–ZrO_2 calcined at various temperatures from 550 to 1200°C has been studied. The calcination at 900°C shows a maximum amount of oxygen-deficient sites on the surface of the catalyst. The synergistic action due to the rhodium localized and/or aggregated on the CeO_2–ZrO_2 surface contributes to the reduction creating surface oxygen vacancy in addition to the considerable change of the CeO_2–ZrO_2 structure.

2. Experimental

Materials. All reagents used were commercial materials of analytical grade. Hydrogen (purity of higher than 99.9%) was used without further purification.

CeO_2–ZrO_2 support. The CeO_2–ZrO_2 support was prepared by precipitation method adding aq. 3 N NH_3 solution to $Ce(NO_3)_3$ and $ZrO(NO_3)_2$ solution up to the pH of 10 slowly. The resulting precipitation was washed with ion-exchanged water, filtered in vacuo, and then dried at 80°C over night. The support was calcined for 3 h at a fixed temperature.

Rh/CeO_2–ZrO_2. In a typical preparation, CeO_2(70 mol%)–ZrO_2(30 mol%), 1.99 g, was impregnated with an aqueous solution of $Rh(NO_3)_3$, 0.026 g, and the water was evaporated using a rotary evaporator. The resulting precipitation was dried for 1 day at 80°C, followed by calcination for 3 h at 550°C to minimize the effect of loading temperature on the support morphology.

X-ray powder diffraction (XRD). XRD patterns of the samples were recorded using a Macscience 18

spectrometer (Ni-filtered Cu K_α, 40 kV–50 mA). The sample was mounted on a sample board and the measurement was carried out immediately. XRD peak positions of the catalysts are corrected using the peak resulting from Si powder as a calibrator.

Reduction of the catalyst with hydrogen. The reduction was carried out by a Cahn electrobalance system. The catalyst, 50 mg, was weighed accurately and evacuated at 400°C till the sample weight became constant. Then the sample was exposed at 400°C to 1.25 kPa of hydrogen, and the reduction extent was measured by the weight loss of the samples when terminating the reduction: desorption of water formed by hydrogen reduction gives the weight loss. The time of introducing hydrogen was the starting point of the reduction. The vapor pressure of formed water was less than 0.02 kPa in the maximum reduction case and its vapor effect on the reduction was negligible.

Surface area. The surface area of the catalysts was determined by the BET method using nitrogen adsorption isotherm at −196°C.

3. Results and discussion

The reduction of rhodium oxides loaded CeO_2(70 mol%)–ZrO_2 calcined at different temperatures was studied. The reduction was completely terminated within 1 h under the conditions. The influence of calcination temperature on the reduction is shown in figure 1. The extent of the reduction of Rh/CeO_2–ZrO_2 increases with an increase in calcination temperature. It is well known that, below 227°C, rhodium oxides loaded on other reducible oxides like TiO_2, Ta_2O_5, and CeO_2 are reduced to the metal by hydrogen [2,13,18,24]. The overweight loss from a stoichiometric value, 2.3 mg/g, indicates that the supports calcined at 800–1200°C are partially reduced, because the theoretical weight loss

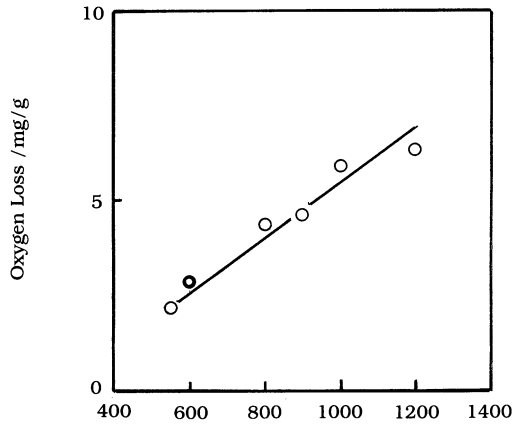

Figure 1. Effect of the calcination temperature on the reduction extent of Rh/CeO_2–ZrO_2. The sample loaded with 1.0 wt% of rhodium was reduced at 400°C under 1.25 kPa of hydrogen pressure.

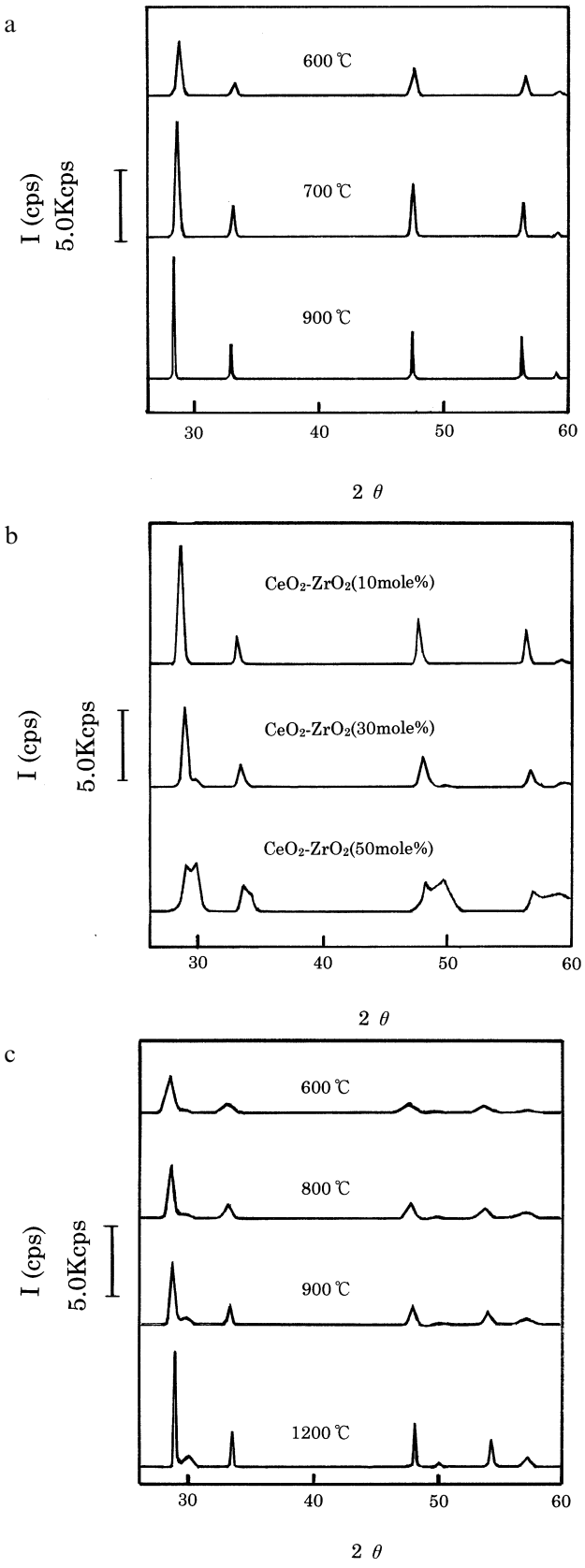

Figure 2. X-ray powder diffraction patterns. All samples were loaded with 1.0 wt% of rhodium. (a) CeO_2 calcined at various temperatures, (b) CeO_2–ZrO_2 containing 10, 30 and 50 mol% of ZrO_2, (c) CeO_2 (70 mol%)–ZrO_2 calcined at various temperatures.

due to reduction of Rh_2O_3 to Rh metal is evaluated to be 2.3 mg/g from its content. The loaded rhodium enhances the reduction remarkably because the support was scarcely reduced with hydrogen in the absence of rhodium.

X-ray powder diffraction patterns of CeO_2, CeO_2–ZrO_2, and Rh_2O_3/CeO_2–ZrO_2 were recorded and shown in figure 2. These XRD patterns were similar to one another except for CeO_2(50 mol%)–ZrO_2 and the load of rhodium oxides had little effect on the XRD patterns of the supports. Furthermore, the peak positions in CeO_2–ZrO_2 shift to higher diffraction angle with an increase in calcination temperature, and those in CeO_2 to a lower one. The sample loaded with more than 4 wt% of rhodium showed the XRD peaks resulting from Rh_2O_3. On the basis of the literature [25], the peaks of the diffraction angles of $2\theta = 29°$, 33°, 48°, 56°, 59°, 70°, 77°, and 78° are attributed to the CeO_2 crystal face of (1, 1, 1), (2, 0, 0), (2, 2, 0), (3, 1, 1), (2, 2, 2), (4, 0, 0), (3, 3, 1), and (4, 2, 0), respectively. Thus, the structure of CeO_2–ZrO_2 crystallites is similar to the fluorite structure of CeO_2 crystal. As shown in figure 2, the peaks resulting from the crystal face of (1, 1, 1), (2, 0, 0), (2, 2, 0), and (3, 1, 1) are clearly narrow. These peaks shift to higher diffraction angle with an increase in ZrO_2 content as shown in figure 2b. This result indicates a dissolution of ZrO_2 in CeO_2. The most of ZrO_2 is dissoluted in CeO_2(90 mol%)–ZrO_2 and CeO_2(70 mol%)–ZrO_2, whereas some parts of ZrO_2 in CeO_2(50 mol%)–ZrO_2 remain without dissolution because the peaks at $2\theta = 30°$, 34° and 50° for CeO_2(50 mol%)–ZrO_2(50 mol%) are assigned to tetragonal ZrO_2 from the literature [27]. The lattice constants for the CeO_2(70 mol%)–ZrO_2 are determinable from the narrow peaks, considering their crystal structures to be fluorite-like structure. The effect of ZrO_2 content and calcination temperature on the lattice constant is shown in figure 3. The lattice constant of CeO_2–ZrO_2 decreases with an increase in ZrO_2 content and that of CeO_2(70 mol%)–ZrO_2 also does with an increase in calcination temperature, while that of CeO_2 increased up to lattice constant of CeO_2 crystal, $a = 0.5411$ nm. The decrease of the lattice constant in CeO_2(70 mol%)–ZrO_2 is reasonably explained in terms of dissolution of zirconium ions, the radius of which is smaller than that of cerium ions [26]. The weak shoulders at the peaks of (1, 1, 1), and (2, 0, 0), and the very weak peak at $2\theta = 50°$ for CeO_2(70 mol%)–ZrO_2 are also attributed to tetragonal ZrO_2. The correlation curve between the lattice constant and the calcination temperature has an inflection point at 900°C.

The crystal size was determined from the half-width of the peaks at (1, 1, 1), (2, 0, 0), (2, 2, 0), and (3, 1, 1) using Scherrer's equation [28]. The growth of the crystal size with calcination temperature is shown in figure 4 for (1, 1, 1), (2, 0, 0), (2, 2, 0), and (3, 1, 1) planes. The crystal size increases with an increase in calcination temperature. The correlation curve between the crystal size of

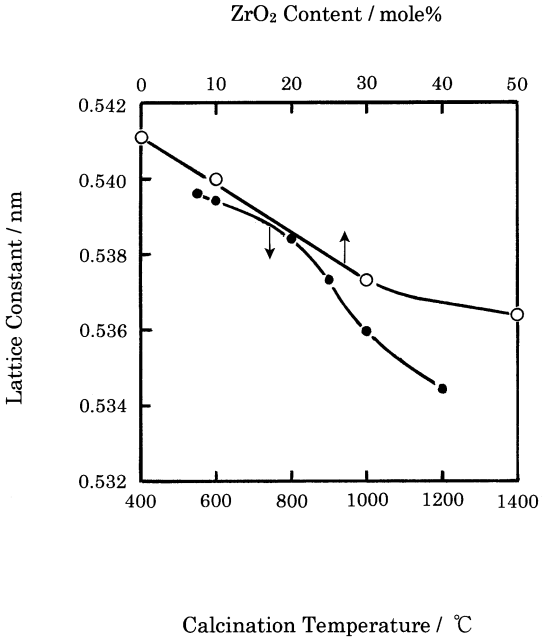

Figure 3. Effect of the content of ZrO_2 and calcination temperature on lattice constant. The lattice constant was calculated from the peak positions of (1, 1, 1), (2, 0, 0), (2, 2, 0) and (3, 1, 1).

CeO_2–ZrO_2 and calcination temperature has also an inflection point at 900°C. These inflection points are well corresponding to the diffusionless tetragonal (t)↔cubic phase (c) transformation in CeO_2(70 wt%)–ZrO_2 around the c↔t equilibrium temperature reported for CeO_2–ZrO_2 crystallites by Yashima et al. [29]. The influence of calcination temperature on the crystal size growth in CeO_2 is much larger than in CeO_2–ZrO_2. This indicates that the dissolution of zirconium ions to CeO_2 depresses the crystal size growth. The crystalline anisotropy of crystal growth is small because the variation of crystal

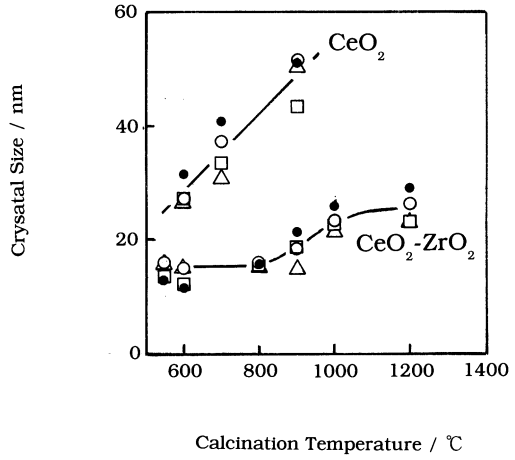

Figure 4. Effect of calcination temperature on crystal growth. (●) Calculated from the (1, 1, 1) peak, (○) calculated from the (2, 0, 0) peak, (□) calculated from the (2, 2, 0) peak, (△) calculated from the (3, 1, 1) peak.

size is little among different crystal faces, as shown in figure 4. The result supports that the CeO_2–ZrO_2 crystallites grow nearly equally to all crystal faces with an increase in calcination temperature under the conditions.

The surface area of the catalysts was measured by the BET method, and the effect of calcination temperature on the surface area is shown in figure 5. The surface area decreases with an increase in calcination temperature. The decrease corresponds well to the growth of the crystal size in figure 4. We have reported that the decomposition of N_2O is catalyzed by oxygen-deficient sites in ceria. The decomposition should occur predominantly on the oxygen-deficient sites in the surface regions of ceria because the adsorption sites of N_2O are present on the surface. It is known that hydrogen reduction at 347–397°C favors the change in surface state from Ce^{4+} to Ce^{3+} with Rh/CeO_2 [2,13,30–32]. From the similarity of the structure of CeO_2–ZrO_2 to that of CeO_2, assuming the surface reduction in Rh/CeO_2–ZrO_2 to occur first of all, the amount of oxygen-deficient sites on the ceria surface is determinable from the surface area, ceria content and oxygen loss shown in figure 1. The number of the CeO_2 unit cell in the surface regions is expressed by an equation, S_{ob}/a^2, where S_{ob} and a are the observed BET surface area and lattice constant of the catalyst, respectively. The number of CeO_2 in the surface regions is expressed by the equation $4 \times 0.70 S_{ob}/a^2$, because a unit cell contains four CeO_2 molecules and the CeO_2 content is 70 mol%. Considering the surface reduction to be $2CeO_2 + H_2 \rightarrow Ce_2O_3 + V_O + H_2O\uparrow$, where V_O is oxygen vacancy, the amount of oxygen-deficient sites creating Ce^{3+} in the surface regions is calculated from $2.8 S_{ob}/2a^2$ and the oxygen loss shown in figure 1, and the plot of the amount vs. calcination temperature is shown in figure 6. Laachir [32], and Shyn [31] reported that the surface reduction occurred in easily reducible surface Ce^{4+} and nonstoichiometric oxides. The amount of oxygen-deficient sites increases up to 900°C and decreases above 900°C with a decrease in surface area. The surface vacancy proceeding N_2O decomposition is a maximum around 900°C. This finding is also consistent with the significant changes of lattice constant and crystal growth at 900°C.

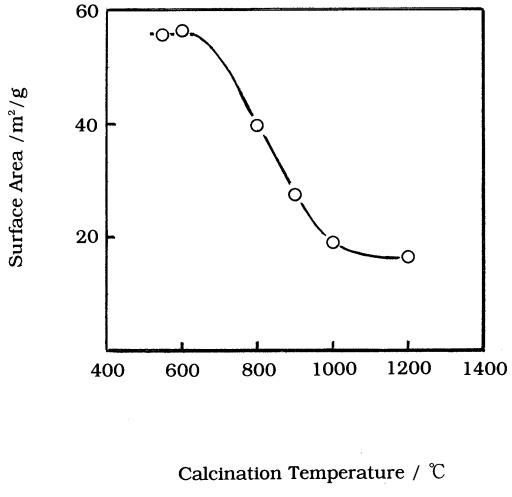

Figure 5. Effect of calcination temperature on the surface area.

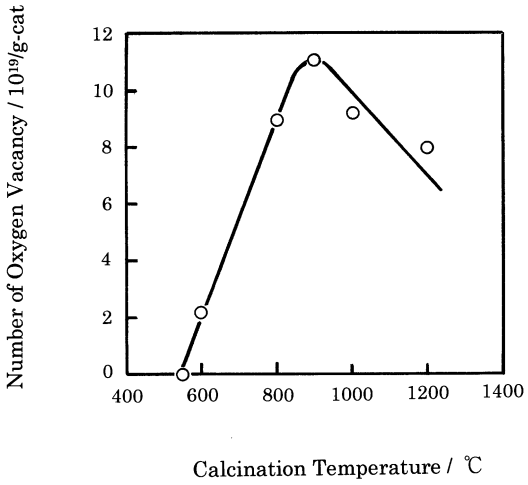

Figure 6. Change of the amount of oxygen-deficient sites in the surface of CeO_2–ZrO_2 with calcination temperature. From the similarity of the CeO_2–ZrO_2 structure to that of CeO_2, assuming that the reduction sets in with an elimination of the lattice oxygen in the surface of the Rh/CeO_2–ZrO_2, the amount of oxygen vacancies in the surface has been calculated.

Assuming the CeO_2–ZrO_2 microlite to be a cube and giving the density of CeO_2(70 wt%)–ZrO_2 to be 6.9 by a proportional allotment of that of CeO_2 (7.3) and ZrO_2 (5.89), the surface area of the catalyst calcined at 550, 900, and 1200°C is calculated mathematically to be 58, 45, and 35 m^2/g respectively from the crystal sizes shown in figure 5. The S_{ob}/S_{cal} ratio is 100% at 550°C, 61% at 900°C, and 50% at 1200°C where S_{ob} is the BET surface area in figure 5. The microlite aggregates with an increase in calcination temperature accompanying the crystal growth: The microlites are separately present at 550–600°C because S_{ob} is equal to the surface area calculated from crystal size of microlite; several microlites may aggregate around 900°C to their crystal texture. About eight microlites may aggregate massively at 1200°C because S_{ob} is equal to the surface area calculated on the basis of the aggregation of eight microlites. The profile of crystal growth is thus illustrated in figure 7.

The contribution of rhodium to the reduction is quite evident because the addition of rhodium remarkably accelerates the reduction. The effect of the rhodium concentration per unit surface area on the extent of reduction was studied to reveal the contribution of the loaded rhodium to the reduction. The amount of hydrogen reduction of Rh/CeO_2–ZrO_2 vs. the rhodium concentration is shown in figure 8. The plot of the reduction amount vs. the rhodium concentration shows a fairly

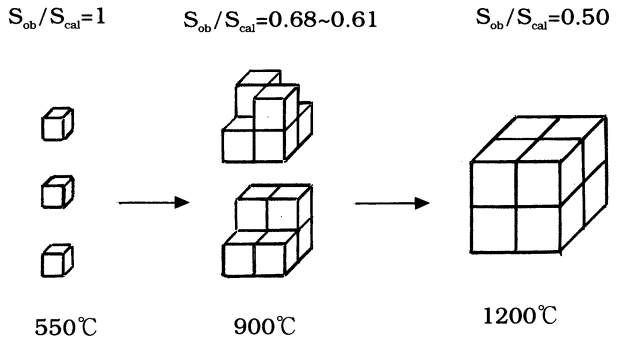

Figure 7. Profile of crystal growth.

near straight line for the catalysts, of which supports have been calcined at various temperatures. Though the hydrogen reduction rate generally depends on the crystalline anisotropy of the crystal face, the overall rate of the hydrogen reduction is not greatly affected by the crystalline anisotropic growth of the crystal face of CeO_2–ZrO_2 crystallites due to different calcination temperatures, because the CeO_2–ZrO_2 crystallites grow nearly equally to all crystal faces with an increase in calcination temperature as described above. In addition, when not only a higher content of cerium in the neighborhood of rhodium but more fine particles of rhodium exist, the rhodium is believed to be more easily diffusible to the ceria; higher surface gives lower rhodium concentration per unit surface and this lower concentration means a higher content of cerium in the neighborhood of rhodium as well as more fine particles of rhodium. A similar diffusion of rhodium was reported for the Rh/CeO_2–ZrO_2 system calcined at higher temperature [11]. In addition, the contribution of the structural change to the reduction should give a curve correlation that has the reflection point. These findings lead to the conclusion that an increase in rhodium concentration significantly accelerates the reduction: the increase accompanies a localization of rhodium with an aggregation of rhodium on the surface; the significant acceleration strongly suggests a synergistic action of the localization and/or the aggregation. The aggregation of rhodium oxides had already been observed in a similar Rh/CeO_2 system [18,33]. Hence, the straight correlation strongly suggests that the localization and/or the aggregation of rhodium means a great deal to enhancing the reduction, that is, a synergistic action due to the localization and/or the aggregation of rhodium facilitates the hydrogen reduction, but a lone rhodium or incorporated rhodium has little promotion for the reduction. The localization and/or the aggregation effect also contributes to the reduction creating the surface oxygen vacancy.

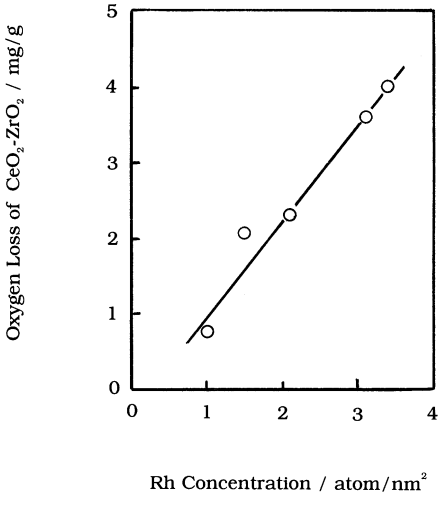

Figure 8. Effect of Rh concentration per unit surface area on the reduction extent. The sample loaded with 1 wt% of rhodium was reduced at 400°C under 1.25 kPa of hydrogen pressure.

4. Conclusion

The lattice constant and the surface area of 70 mol% CeO_2–ZrO_2 decrease with an increase in calcination temperature and significantly change around 900°C, whereas the crystal size increases with an increase in calcination temperature and significantly changes around 900°C. These findings indicate that the structure of CeO_2–ZrO_2 changes with an increase in calcination temperature and significantly changes around 900°C. Moreover, the plot of the reduction amount vs. the rhodium concentration shows a fairly near straight line in addition to the considerable structure change of CeO_2–ZrO_2. The straight correlation strongly suggests that a synergistic action due to the localization and/or the aggregation of rhodium enhances the hydrogen reduction of CeO_2–ZrO_2, but a lone rhodium and/or incorporated rhodium has little promotion for the reduction.

References

[1] J.C. Summers and A. Ausen, J. Catal. 58 (1979) 131.
[2] H.C. Yao and Y.F. Yu Yao, J. Catal. 86 (1984) 254.
[3] E.C. Su, C.N. Montereuil and W.G. Rothschild, Appl. Catal. 17 (1985) 75.
[4] S.H. Oh and C.C. Eickel, J. Catal. 112 (1988) 543.
[5] B.H. Engler, E. Koberstein and P. Schubert, Appl. Catal. 48 (1989) 71.
[6] P. Loof, B. Kasemo and K.E. Keck, J. Catal. 118 (1989) 339.
[7] T. Miki, T. Ogawa, M. Haneda, N. Kakuta, A. Ueno, S. Tateishi, S. Matsuura and M. Sato, J. Phys. Chem. 94 (1990) 339.
[8] S.H. Oh, J. Catal. 124 (1990) 477.
[9] J.G. Numan, H.J. Robota, M.J. Cohn and S.A. Bradley, J. Catal. 133 (1992) 309.
[10] C. Padeste, N.W. Cant and D.L. Trimm, Catal. Lett. 18 (1993) 305.
[11] G.S. Zafiris and R.J. Gorte, J. Catal. 143 (1993) 86.
[12] S. Imamura, M. Shono, N. Okamoto, A. Hamada and S. Ishida, Appl. Catal. A 142 (1996) 279.

[13] B. Harrison, A.F. Diwell and C. Hallett, Platinum Metals Rev. 32 (1988) 73.
[14] A. Cook, A.G. Fitzgerald and J.A. Cairns, in: *Catalysis and Surface Characterization*, eds. T.J. Dines, C.H. Rochester and J. Thomson (Royal Society of Chemistry, Cambridge, 1992) p. 249.
[15] F.L. Normand, L. Hilaire, K. Kili and G. Maire, J. Phys. Chem. 92 (1988) 2561.
[16] J.T. Kummer, Y. Yao and D. McKee, SAE Paper No. 760143 (1976).
[17] E. Tani, M. Yoshimura and S. Somiya, J. Am. Ceram. Soc. 66 (1983) 506.
[18] G. Ranga Rao, J. Kasper, S. Meriani, R. Di Monte and M. Graziani, Catal. Lett. 24 (1994) 107;
P. Fornasiero, R. Di Monte, G. Ranga Rao, J. Kasper, S. Meriani, A. Trovarelli and M. Graziani, J. Catal. 151 (1995) 168;
P. Fornasiero, G. Balducci, R. Di Monte, J. Kasper, V. Sergo, G. Gubitosa, A. Ferrero and M. Graziani, J. Catal. 164 (1996) 174.
[19] P. Duran, M. Gonzalez, C. Moure, J.R. Jurdo and C. Pascal, J. Mater. Sci. 25 (1990) 5001.
[20] S. Meriani, Mater. Sci. Eng. A 109 (1989) 121.
[21] B.K. Cho, J. Catal. 131 (1991) 74.
[22] C. Serre, F. Garin, G. Belot and G. Maire, J. Catal. 141 (1993) 1.
[23] S. Imamura, N. Okamoto, Y. Saito, T. Ito and H. Jindai, *J. The Japan Petroleum Institute* 39 (1996) 350;
S. Imamura, T. Kitao, H. Kanai, S. Shono, K. Utani and H. Jindai, React. Kinet. Catal. Lett. 61 (1997) 201.
[24] J. Cunningham, D. Cullinane, J. Sanz, J.M. Rojo, X.A. Soria and J.L.G. Fierro, J. Chem. Soc. Faraday Trans. 88 (1992) 3233.
[25] Teufer, Acta Cryst. 15 (1962) 1187; JCPDS 24-1164.
[26] R.D. Shannon, Acta Cryst. A 32 (1976) 751.
[27] Dragoo and Domingues, Nat. Bur. Stand. (US) Monogr. 20 (1983) 38; JCPDS 34-394.
[28] P. Scherrer, Göttinger Nachrichten 2 (1918) 98.
[29] M. Yashima, K. Morimoto, N. Ishizawa and M. Yoshimura, J. Am. Ceram. Soc. 76 (1993) 2865;
M. Yashima, H. Arashi, M. Kakihana and M. Yoshimura, J. Am. Ceram. Soc. 77 (1994) 1067.
[30] M.F.L. Johnson and J. Mooi, J. Catal. 103 (1987) 502.
[31] J.Z. Shyn, W.H. Weber and H.S. Gandhi, J. Phys. Chem. 92 (1988) 4964.
[32] A. Laachir, V. Perrichon, A. Badri, J. Lamotte, E. Catherine, J.C. Lavalley, J.E. Fallah, L. Hilaire, F. Le Normand, E. Quémére, G.N. Sauvion and O. Touret, J. Chem. Soc. Faraday Trans. 87 (1991) 1601;
V. Perrichon, A. Laachir, G. Bergeret, R. Fréty, L. Tournayan and O.J. Tóuret, J. Chem. Soc. Faraday Trans. 90 (1994) 773.
[33] J.C. Vis, H.F.J. van 't Blik, T. Huizinga, J. van Grondelle and R. Prins, J. Catal. 95 (1985) 333.